Chapter 5

Enhanced Distillation Under Infrared Characteristic Radiation

Kuo-Ting Wang, M. Quinn Brewster and
Wei-Hsiang Lai

Additional information is available at the end of the chapter

http://dx.doi.org/10.5772/67401

Abstract

This chapter introduces quasi-steady water vaporization under mid-infrared (IR) radiation and the IR absorption of characteristic radiation associated with the first-kind liquid-gaseous phase transition of water. When characteristic radiation in the mid-IR spectral range is applied to water surface, the strong volumetric absorption of radiation energy in the liquid-phase causes water to be nearly isothermal. In addition to volumetric absorption, surface absorption of characteristic radiation induces vaporization of water. The complete mechanism of liquid-gaseous phase-transition radiation involves the direct surface absorption/emission of infrared energy accompanied by evaporation/condensation of water. A direct consequence of excess characteristic radiation upon water surface is the induced supersaturation. This mechanism opens up a door for enhanced distillation under characteristic radiation. Blackbody-like materials such as black anodized aluminum surfaces and metal surfaces painted in black are recommended to be heated to ~250°C to serve as economical radiation sources. For isothermal water at room temperatures, ~20% supersaturation can be induced by hemispherical Blackbody radiation with temperature ~11°C higher than the water temperature. In this situation, energy extracted from the ambient for water vaporization can be as much as 80% of latent heat. With radiation-enhanced evaporation, the production cost for distilled water is significantly reduced as compared to distillation at the boiling point.

Keywords: water, evaporation, supersaturation, infrared, radiation, phase-transition radiation

1. Introduction

While latent heat of evaporation is a fixed amount of energy needed to vaporize liquid-water, how energy is supplied to cause evaporation is an open area for engineers to explore to achieve their design goals. Evaporation is a process that water molecules go through the phase transition of the first kind from the liquid phase to the gaseous phase. This process is driven by the concentration gradient of water molecules on the vapor side of the water surface. When water is heated up to the boiling point, the saturation pressure of water is increased to exceed the ambient water-vapor pressure not only on the water surface but also in the bulk so that "evaporation" (*boiling*) takes place everywhere in the water. For water purification purposes, water can be distilled in this way. One advantage of this type of water purification is that distillation can be quickly carried out by supplying sufficient heat. However, one obvious disadvantage at the same time is that a significant amount of energy is lost to the ambient in order to maintain water temperature at the boiling point.

This chapter suggests another way of distillation that enables water to be supersaturated on the surface so as to enhance evaporation. This method utilizes the mechanism of so-called phase-transition radiation to enhance evaporation without requiring water to reach the boiling point. Since liquid-water molecules are constantly experiencing breaking and formation of hydrogen bonds due to intermolecular vibrations, there are moments when some water molecules are weakly bonded. When photons hit such molecules on the surface, the photons that carry enough energy to break the hydrogen bond will be absorbed to cause transitions of energy states, namely evaporation. The spectral range of the evaporative absorption defines the spectrum of characteristic radiation, which is in the mid-IR range. A good amount of effort [1] has been spent on the characteristic wavelength of phase-transition radiation in vapor condensation process.

Quasi-steady equations for radiation absorption in semi-infinite liquid-water as well as their dilute approximations are presented in this chapter. Semi-infinite liquid-water is selected to represent a common scenario for engineering distillation applications. These equations deal with liquid phase, vapor phase, and the vapor liquid interface in the presence of IR characteristic radiation. In addition to volumetric absorption of radiation, which is commonly recognized as far as radiative heat transfer is concerned, surface absorption of radiation is taken into account in the liquid-phase equations. Based on the IR absorption characteristics in the liquid-water, the liquid phase is essentially isothermal under moderate radiation strength in the mid-IR range. In the equations for vapor phase and interface, the situation of supersaturation triggered by an excess amount of IR characteristic radiation is presented for the first time. Enhanced evaporation as a result of supersaturation is exemplified in dilute systems. Although the enhanced evaporation rate by IR radiation may not be as fast as that of the traditional way of boiling water, this method is more energy efficient and economical when continual distillation is needed for a larger amount of water.

In the last section of this chapter, the theory of phase-transition radiation is extended to the situation of supersaturation for semi-infinite water. The evaporation flux due to phase-transition radiation is linked to characteristic radiation and supersaturation. The equation for

http://dx.doi.org/10.5772/67401

quasi-steady supersaturation is obtained and used to close the mathematic problem when vapor pressure at water surface is no longer subject to saturation conditions.

2. Quasi-steady semi-infinite water

2.1. Liquid phase

A sketch for the thermodynamic system of semi-infinite water is shown in **Figure 1**. In the liquid phase, the temperature distribution is subject to three heat transfer modes: conduction, convection, and radiation,

$$q = -k_l \frac{dT}{dx} - \dot{m}'' C\left(T + T_{ref}\right) + \left(1 - f_s\right) q_r \tag{1}$$

where q denotes heat flux, k_l thermal conductivity of liquid-water, $\dot{m}''$ mass flux, C heat capacity of water, f_s the fraction of surface absorption of radiation, and q_r radiative heat flux. Surface absorption efficiency f_s is defined later in Section 2.4 and its values ($0 \le f_s \le 1$) are plotted in **Figure 6**.

A general temperature equation can be obtained by imposing constant heat flux conditions at quasi-steady state with respect to water depth (i.e., x-direction in **Figure 1**),

$$\frac{dq}{dx} = 0 \Rightarrow k_l \frac{d^2T}{dx^2} + \dot{m}'' C \frac{dT}{dx} - \left(1 - f_s\right) \frac{dq_r}{dx} = 0 \tag{2}$$

For the radiative heat transfer with absorption coefficient K_a in liquid-water,

$$\frac{dq_r}{dx} = -K_a q_r \Rightarrow q_r = q_{r,s} e^{-K_a x} \Rightarrow \frac{dq_r}{dx} = -q_{r,s} K_a e^{-K_a x}, \tag{3}$$

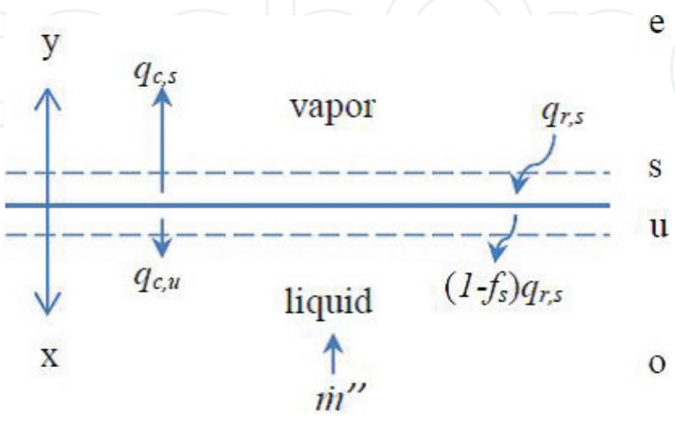

Figure 1. Definitions for thermodynamic states, energy fluxes, and coordinate systems at vapor-liquid interface for semi-infinite water.

which leads to

$$k_l \frac{d^2T}{dx^2} + \dot{m}'' C \frac{dT}{dx} + \left(1 - f_s\right) q_{r,s} K_a e^{-K_a x} = 0. \tag{4}$$

Temperature boundary conditions (BCs) at surface (i.e., T_s at $x = 0$) and at a sufficiently deep location (either T at $x \to \infty$ or $dT/dx = 0$ at $x \to \infty$) can be specified to solve Eq. (4).

BCs: $T|_{x=0} = T_s$, $\left.\frac{dT}{dx}\right|_{x\to\infty} = 0$ or $T|_{x\to\infty} = T_o$.

2.1.1. Nondimensionalization

For small temperature changes (i.e., a few degrees C), physical properties (K_a, k_l, C, f_s) can be assumed to be constant and a general form for the liquid-phase equation is obtained following a nondimensionalization analysis with,

$$\begin{aligned} &\delta_r = 1/K_a, \qquad \delta_t = k_l/\left(\dot{m}'' C\right), \qquad \overline{x} = x/\delta_r, \\ &\Delta T_{\max} = \left(1 - f_s\right) q_{r,s} / \left[k_l \left(\delta_r{}^{-1} - \delta_t{}^{-1}\right)\right], \qquad \overline{T} = (T - T_s)/\Delta T_{\max}, \\ &\frac{d^2\overline{T}}{d\overline{x}^2} + \frac{\delta_r}{\delta_t}\frac{d\overline{T}}{d\overline{x}} + \left(1 - \frac{\delta_r}{\delta_t}\right) e^{-\overline{x}} = 0. \end{aligned} \tag{5}$$

In Eq. (5) different scales for length (characteristic length for IR absorption δ_r and convective length scale δ_t) as well as temperature (ΔT_{max}) [2] are used to formulate the nondimensional form. Based on two different kinds of BCs, two different forms of solutions are obtained,

General solution: $\overline{T} = A + Be^{-\overline{x}(\delta_r/\delta_t)} - e^{-\overline{x}}$ (A, B: constants);

Case 1: BCs $\overline{T}\big|_{\overline{x}=0} = 0$, $\left.\frac{d\overline{T}}{d\overline{x}}\right|_{\overline{x}\to\infty} = 0$, solution: $\overline{T} = e^{-\overline{x}(\delta_r/\delta_t)} - e^{-\overline{x}}$;

Case 2: BCs $\overline{T}\big|_{\overline{x}=0} = 0$, $\overline{T}\big|_{\overline{x}\to\infty} = (T_o - T_s)/\Delta T_{\max} = \overline{T_o}$, solution: $\overline{T} = \overline{T_o} + \left(1 - \overline{T_o}\right) e^{-\overline{x}(\delta_r/\delta_t)} - e^{-\overline{x}}$.

2.1.2. Isothermal water under mid-IR

Based on the mid-IR absorption spectrum of liquid-water, water is fairly opaque under mid-IR radiation and the attenuation of mid-IR radiation occurs within only several microns [2]. The characteristic length for IR absorption δ_r (which is inversely proportional to the absorption coefficient) is much smaller than the convective length scale of water δ_t in typical conditions. As a result, the convection term in the liquid-phase temperature equation can be ignored. The simplified equation has the following form,

$$\frac{\delta_r}{\delta_t} \approx 0 \Rightarrow \frac{d^2\overline{T}}{d\overline{x}^2} + e^{-\overline{x}} \approx 0, \quad \Delta T_{\max} \approx \left(1 - f_s\right) q_{r,s} \delta_r / k_l, \tag{6}$$

and the same simplified solution for both Cases 1 and 2,

$$\overline{T} \approx 1 - e^{-\overline{x}} \text{ or } T \approx T_s + \Delta T_{\max}\left(1 - e^{-K_a x}\right). \tag{7}$$

Eq. (7) leads to an important feature for liquid-phase quasi-steady temperature distribution: water is essentially isothermal under mid-IR radiation with moderate strength [2], as illustrated in Example 1.

The liquid-phase enthalpy changes from the top ($x = 0$) to the bottom ($x \to \infty$) can be described in terms of conductive and radiative heat transfer by applying integration to Eq. (4) from $x = 0$ to $x \to \infty$:

$$k_l \left.\frac{dT}{dx}\right|_{x=0}^{x\to\infty} + \dot{m}'' CT\big|_{x=0}^{x\to\infty} - \left(1 - f_s\right) q_{r,s} e^{-K_a x}\big|_{x=0}^{x\to\infty} = 0 \Rightarrow \left(q_{c,u} - q_{c,o}\right)$$
$$+ \dot{m}''\left(h_{1,o} - h_{1,u}\right) + \left(1 - f_s\right) q_{r,s} = 0.$$

Normally the temperature gradient vanishes at the bottom, $q_{c,o} = 0$, giving,

$$\dot{m}''\left(h_{1,o} - h_{1,u}\right) = -\left(1 - f_s\right) q_{r,s} - q_{c,u}. \tag{8}$$

2.2. Vapor phase

Basic definitions related to water vapor-air mixtures in the vapor phase are reviewed before introducing vapor-phase equations. We shall limit our discussions to two-species mixtures.

2.2.1. Basic definitions

$$h = m_1 h_1 + m_2 h_2 \qquad \text{(mixture enthalpy)}$$
$$C_p = m_1 C_{p,1} + m_2 C_{p,2} \qquad \text{(mixture } C_p\text{)}$$
$$\rho = \rho_1 + \rho_2 \qquad \text{(mixture density)}$$
$$m_{1,2} = \frac{\rho_{1,2}}{\rho} \qquad \text{(mass fraction of species 1, vapor or 2, air)}$$

Assuming ideal gas for water vapor and air, vapor mass fraction m_1 becomes,

$$m_1 = \frac{\rho_1}{\rho} = \frac{P_1 M_1}{P_1 M_1 + P_2 M_2} = \frac{P_1}{\frac{M_2}{M_1} P + \left(1 - \frac{M_2}{M_1}\right) P_1} = \frac{(RH) P_{sat}}{1.61P - 0.61(RH) P_{sat}}, \tag{9}$$

where the ratio of air molecular weight to vapor, $M_2/M_1 = 28.97/18 = 1.61$, and the partial pressure of vapor $P_1 = (RH)\ (P_{sat})$. This form of m_1 and its dilute approximation are listed in **Table 3**. Reference values for air molecular weight and other properties are available at [3].

2.2.2. Mass transfer of water vapor

The transport of water vapor can be divided into two parts: the microscopic molecular diffusion and the macroscopic convection. When vapor mass fraction is much less than unity, i.e., $m_1 << 1$, the macroscopic convection term is often negligible, leaving the diffusion term described by Fick's law in the dilute system. Mass flux of water vapor is described by,

$$\dot{m}_1'' = \underbrace{m_1 \rho v}_{convection} \underbrace{-\rho D \frac{dm_1}{dy}}_{diffusion}. \tag{10}$$

The quasi-steady equation for vapor mass transport is obtained assuming constant D,

$$\frac{d\left(\dot{m}_1''\right)}{dy} = 0 \Rightarrow \rho D \frac{d^2 m_1}{dy^2} = \rho v \frac{dm_1}{dy}. \tag{11}$$

The algebraic formula for mass diffusivity D is listed in **Table 1**.

Output	Input	Algebraic formula	Max error	Reference
T_{sat} [°C]	P_{sat} [atm]	$T_{sat} = \frac{237.3 \times \log_{10}\left(\frac{P_{sat}}{0.00603}\right)}{7.5 - \log_{10}\left(\frac{P_{sat}}{0.00603}\right)}$	<1%	[4]
P_{sat} [atm]	T_{sat} [°C]	$P_{sat} = 0.00603 \times 10^{\frac{7.5 T_{sat}}{237.3 + T_{sat}}}$	<1%	[4]
D [m^2/s]	P [atm], T [°C]	$D = \left(1.97 \times 10^{-5}\right)\left(\frac{273.15+T}{256}\right)^{1.685}\left(\frac{1.013}{P}\right)$		[2]
α_{sat} [m^2/s]	T [°C]	$\alpha_{sat} = \sum_{i=0}^{4} SA_i T_i^{\,i}$		[5]
α_{dry} [m^2/s]	k [W/m-K], ρ [g/m^3], C_p [kJ/kg-K]	$\alpha_{dry} = \frac{k}{\rho C_p}$		Definition
k [W/m-K]	T [K]	$k = \sum_{i=0}^{5} KA_i T_i^{\,i}$		[5]
$C_{p,2}$ [kJ/kg-K]	T [K]	$C_{p,2} = \sum_{i=0}^{4} CA_i T_i^{\,i} \approx 1$		[5]
ρ_2 [g/m^3]	P [Pa], T [K]	$\rho_2 = \frac{PM_{air}}{RT}$		Ideal gas
h_2 [kJ/kg]	T [°C]	$h_2 = 2501 + T$		
$h_{1,u}$ [kJ/kg]	T [°C]	$h_{1,u} = 4.2T$	<1%	

Errors are based on comparisons with available data from steam tables for T = 1–100°C.

Table 1. Algebraic formulae for selected properties.

2.2.3. Heat transfer in water vapor-air mixtures

For the mixture heat flux, conduction is included in addition to diffusion and convection,

$$q = \underbrace{\rho v h}_{convection} \underbrace{-\rho D \sum_{i=1}^{2} h_i \frac{dm_i}{dy}}_{diffusion} \underbrace{-k \frac{dT}{dy}}_{conduction} = \left(\rho v h - \rho \frac{k}{\rho C_p} \frac{dh}{dy}\right) + \sum_{i=1}^{2} h_i \frac{dm_i}{dy}\left(\rho \frac{k}{\rho C_p} - \rho D\right). \tag{12}$$

http://dx.doi.org/10.5772/67401

In the two-species system, since $m = m_1 + m_2 = 1$ = constant, it follows that $dm_2 = -dm_1$, and,

$$q = \left(\rho v h - \rho\alpha \frac{dh}{dy}\right) - \left(\rho D \frac{dm_1}{dy}\right)(h_1 - h_2)\left(1 - \frac{1}{Le}\right), \tag{13}$$

where Lewis number $Le = D/\alpha$ and thermal diffusivity $\alpha = k/\rho C_p$. Numerical values of Le for dry air and saturated air at different temperatures are tabulated in **Table 4** and plotted in **Figure 2**. The algebraic formula for α can be found in **Table 1** with the corresponding curve-fit coefficients available in **Table 2** [5].

The heat flux equation can be simplified if any of the following conditions are valid: (1) dilute; (2) nearly equal enthalpy for two species; (3) $Le \approx 1$, which is generally true for air-vapor mixtures under atmospheric conditions. The condition of nearly equal enthalpy is achievable with properly chosen reference enthalpies for air and vapor. To achieve this condition, enthalpies of liquid-water and vapor are taken from steam tables and the reference enthalpy of air is set to $h_{2,ref}$ = 2501 kJ/kg at T_{ref} = 0°C to give,

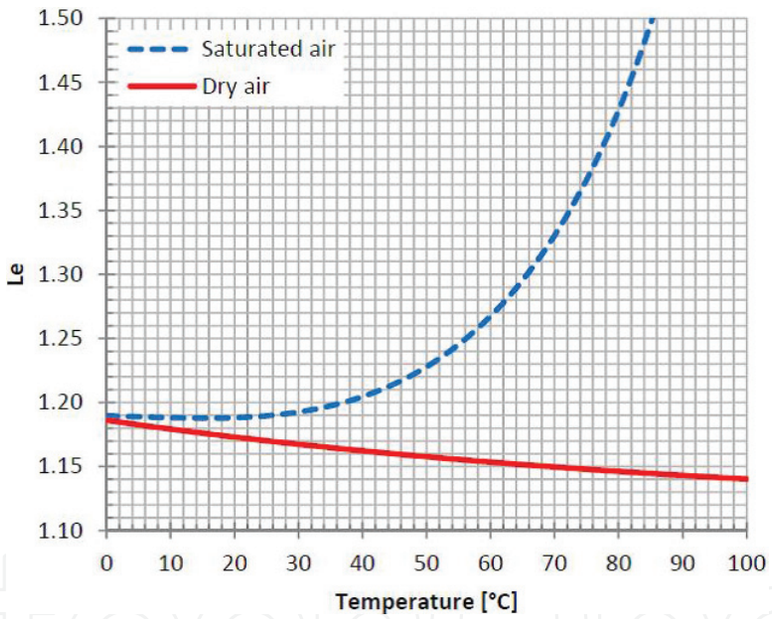

Figure 2. Lewis number, *Le*, for saturated air and dry air at one atmosphere. Numerical values are shown in **Table 4**.

α_{sat} [m²/s]	k [W/m-K]	$C_{p,2}$ [kJ/kg-K]	ρ [g/m³]
SA_0 = 1.847185729E-5	KA_0 = −2.276501E-3	CA_0 = 1.03409	M_{air} = 28.97 [g/mol] [3]
SA_1 = 1.161914598E-7	KA_1 = 1.2598485E-4	CA_1 = −2.84887E-4	R = 8.314 [J/mol-K]
SA_2 = 2.373056947E-10	KA_2 = −1.4815235E-7	CA_2 = 7.816818E-7	
SA_3 = −5.769352751E-12	KA_3 = 1.73550646E-10	CA_3 = −4.970786E-10	
SA_4 = −6.369279936E-14	KA_4 = −1.066657E-13	CA_4 = 1.077024E-13	
	KA_5 = 2.47663035E-17		

Table 2. A supplemental table with numerical coefficients and constants for **Table 1**.

Variable	Original form	Algebraic formula	Dilute approximation (m_1<<1)
m_1	$\frac{\rho_1}{\rho}$	$\frac{(RH)P_{sat}}{1.61P-0.61(RH)P_{sat}}$	$\frac{(RH)P_{sat}}{1.61P}$
$\dot{m}''$	$\frac{\rho D}{L}\ln(1+B_m)$	$\frac{\rho D}{L}\ln\left(1+\frac{m_{1,s}-m_{1,e}}{1-m_{1,s}}\right)$	$\rho D\frac{m_{1,s}-m_{1,e}}{L}$; $\frac{\rho D}{L}\frac{(RH)_sP_{sat,s}-(RH)_eP_{sat,e}}{1.61P}$
$\dot{m}''$	$\frac{\rho\alpha}{L}\ln(1+B_h)$	$\frac{\rho\alpha}{L}\ln\left[1+\frac{h_e-h_s}{h_s-\left(h_{1,o}+q_{r,s}/\dot{m}''\right)}\right]$	$\frac{\rho\alpha}{L}\frac{C_p\left(T_e-T_s+T_{r,s}\right)}{\left(h_s-h_{1,o}\right)}$, $T_{r,s}=\frac{q_{r,s}L}{k}$
C_p	$m_2C_{p,1}+m_2C_{p,2}$		$C_{p,2}$
H	$m_1h_1+m_2h_2$		h_2

Table 3. Different forms of selected variables and their dilute approximations.

$$h_2[\text{kJ/kg}] = h_{2,ref} + C_{p,2}T\ \ [^\circ\text{C}] \approx 2501 + T\ \ [^\circ\text{C}], \tag{14}$$

where $C_{p,2} \approx 1$ kJ/kg-K for $T = 0$–100°C. The liquid-water enthalpy is approximated (within 1% errors for $T = 1$–99°C as compared to steam tables) by,

$$h_{1,u}[\text{kJ/kg}] \approx 4.2T\ \ [^\circ\text{C}]. \tag{15}$$

This leads to a simplified heat flux equation,

$$q \approx \left(\rho vh - \rho\alpha\frac{dh}{dy}\right), \tag{16}$$

and its quasi-steady equation,

$$\frac{dq}{dy} = 0 \Rightarrow \rho\alpha\frac{d^2h}{dy^2} \approx \rho v\frac{dh}{dy}. \tag{17}$$

Dilute approximations for mixture enthalpy h and specific heat C_p are listed in **Table 3**. Algebraic forms for air enthalpy h_2 and specific heat $C_{p,2}$ are tabulated in **Table 1**. Curve-fit coefficients for $C_{p,2}$ are placed in **Table 2** [5].

2.3. Vapor-liquid interface

Vapor-liquid interface equations are obtained by matching the mass flux of species 1 (vapor or liquid-water) and energy flux at the interface.

Mass flux of species 1:

$$\dot{m}'' = \overbrace{\dot{m}_u''}^{liquid} = \dot{m}_{1,u}'' = \overbrace{\dot{m}_{1,s}'' = \underbrace{m_{1,s}\rho v}_{convection} - \underbrace{\rho D\left.\frac{dm_1}{dy}\right|_s}_{diffusion}}^{vapor} = m_{1,s}\dot{m}'' - \rho D\left.\frac{dm_1}{dy}\right|_s$$

$$\Rightarrow \dot{m}'' = -\frac{\rho D}{1-m_{1,s}}\left.\frac{dm_1}{dy}\right|_s. \tag{18}$$

http://dx.doi.org/10.5772/67401

Together with the mass diffusion equation (11), mass flux can be solved for,

$$\dot{m}'' = \frac{\rho D}{L}\ln(1+B_m), \quad B_m = \frac{m_{1,s}-m_{1,e}}{1-m_{1,s}}. \tag{19}$$

Its dilute approximation is listed in **Table 3**.

Heat flux:

$$q = q_u = \overbrace{\underbrace{-q_{c,u}}_{conduction} + \underbrace{\dot{m}'' h_{1,u}}_{convection} + \underbrace{f_s q_{r,s}}_{radiation}}^{liquid} = \overbrace{q_s \approx \dot{m}'' h_s - \rho\alpha \left.\frac{dh}{dy}\right|_s}^{vapor}$$

$$\Rightarrow \dot{m}'' \left[h_s - \left(h_{1,u} - \frac{q_{c,u}}{\dot{m}''} + \frac{f_s q_{r,s}}{\dot{m}''} \right) \right] \approx \rho\alpha \left.\frac{dh}{dy}\right|_s. \tag{20}$$

Eq. (20) is based on enthalpy formulation. Alternatively, the heat flux equation can be obtained based on temperature formulation without approximations,

$$q = q_u = \overbrace{\underbrace{-q_{c,u}}_{conduction} + \underbrace{\dot{m}'' h_{1,u}}_{convection} + \underbrace{f_s q_{r,s}}_{radiation}}^{liquid} = \overbrace{q_s = \dot{m}'' h_{1,s} - k \left.\frac{dT}{dy}\right|_s}^{vapor}$$

$$\Rightarrow \dot{m}'' h_{fg} = \dot{m}'' \left(h_{1,s} - h_{1,u} \right) = -q_{c,u} + f_s q_{r,s} + k \left.\frac{dT}{dy}\right|_s. \tag{21}$$

Based on Eq. (20) and the heat diffusion equation (17), an alternative form for mass flux can be obtained to relate it to heat transfer variables,

$$\dot{m}'' \approx \frac{\rho\alpha}{L}\ln(1+B_h), \qquad B_h = \frac{h_e - h_s}{h_s - \left(h_{1,u} - \frac{q_{c,u}}{\dot{m}''} + \frac{f_s q_{r,s}}{\dot{m}''} \right)}. \tag{22}$$

At the first glance evaporation flux in Eq. (22) seems to be influenced by f_s. However, its dependency on f_s is eliminated [2] when the energy balance for the entire liquid is taken into account as done in Example 2, giving,

$$B_h = \frac{h_e - h_s}{h_s - \left(h_{1,o} + q_{r,s}/\dot{m}'' \right)}. \tag{23}$$

The corresponding dilute approximation for mass flux is shown in **Table 3**.

Given $(RH)_e$, these two forms of mass flux are instrumental in evaluating surface temperature T_s—even without the knowledge of the vapor layer thickness L. For an isothermal dilute system (see approximated forms in **Table 3**), an implicit form for T_s is obtained by equating the two mass-flux forms, giving,

$$\frac{(RH)_s P_{sat,s} - (RH)_e P_{sat,e}}{1.61P(T_e - T_s + T_{r,s})} \approx \frac{C_p}{Le} \frac{1}{\underbrace{2501 + T_s}_{h_s} - \underbrace{4.2T_s}_{h_{1,u}}}, \tag{24}$$

or,

$$\frac{P_{sat,s}}{P} \approx \frac{P_{sat,e}}{P} \frac{(RH)_e}{(RH)_s} + \frac{1.61C_p}{(RH)_s Le} \frac{(T_e - T_s + T_{r,s})}{2501 - 3.2T_s}, \tag{25}$$

in which the unit for temperature (i.e., for T_e, T_s, and $T_{r,s}$) is [°C]. **Figure 2** shows the relationship of Lewis number *Le* with *T* and *RH* at one atmosphere. For evaporation taking place at a moderate-temperature (0–40°C) under atmospheric conditions, $Le \approx 1.18$ appears to be a good approximation for water vapor-air mixtures.

To facilitate numerical calculations, algebraic formulas for thermal properties are listed below.

2.4. Supersaturation by characteristic radiation

2.4.1. Energy distributions of water molecules in gaseous and liquid phases

Unlike conventional two-energy-level models characterized by discrete absorption lines, phase-transition radiation is accompanied by a continuous absorption band. The "band" feature of the characteristic radiation is primarily a result of the convolution of population distributions for translational energy and rotational energy of vapor molecules. Since vapor molecules can be treated as a continuum in atmospheric conditions, the population distribution of translational energy at thermodynamic equilibrium is described by the Maxwell-Boltzmann distribution. Consequently vapor molecules are continuously populated as demonstrated in **Figure 3**. Descriptions for this model can be found in [1]. Intermolecular vibrations of water molecules in the liquid phase broaden the characteristic radiation band and smooth out its far wings.

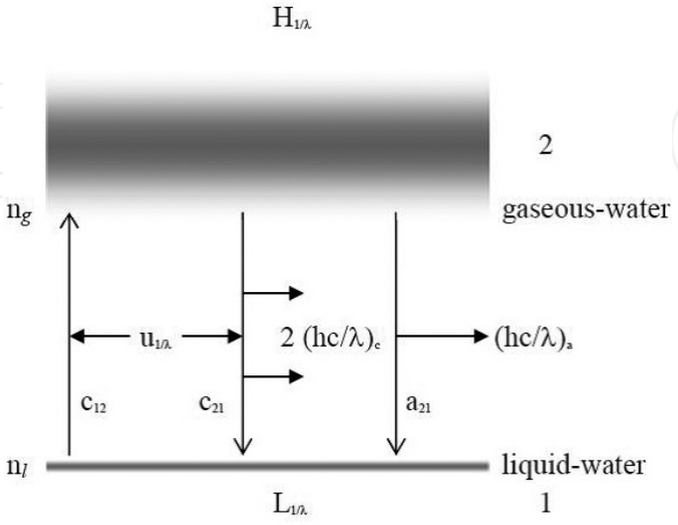

Figure 3. Energy states (2: gaseous; 1: liquid) and phase-transition radiation in the condensation/evaporation process.

http://dx.doi.org/10.5772/67401

Although the peak value of the population distribution function is slightly brought down as a result of the broadening at the lower energy state, a previous work [6] has shown that the shapes of population distributions with and without invoking broadening effects of intermolecular vibrations in liquid-water are similar to each other.

For modeling purposes, vapor molecules are distributed over a continuous band by energy convolution and liquid-water molecules are treated as at the same energy level to simplify mathematical formulations. In other words, the broadening of the lower energy state is ignored. Modeling intermolecular vibrations of water molecules is in fact a very challenging task because the hydrogen bonds, which directly affect intermolecular vibrations, are constantly breaking and forming and are highly dependent on temperature.

Since mathematical forms for population distribution functions for vapor molecules have been established in the previous work [6], their derivations are skipped in this chapter. Together with population distribution functions and related parameters, equations for evaporation fluxes related to absorption, spontaneous emission, and induced emission are outlined in **Table 5**.

T [°C]	Dry air, α_{dry} [m^2/s]	Saturated air, α_{sat} [m^2/s]	D [m^2/s]	Dry air, Le	Saturated air, Le
0	1.853E-05	1.847E-05	2.197E-05	1.186	1.190
1	1.865E-05	1.859E-05	2.211E-05	1.185	1.189
2	1.878E-05	1.871E-05	2.225E-05	1.185	1.189
3	1.891E-05	1.882E-05	2.238E-05	1.184	1.189
4	1.903E-05	1.894E-05	2.252E-05	1.183	1.189
5	1.916E-05	1.906E-05	2.266E-05	1.183	1.189
6	1.929E-05	1.918E-05	2.279E-05	1.182	1.189
7	1.941E-05	1.929E-05	2.293E-05	1.181	1.188
8	1.954E-05	1.941E-05	2.307E-05	1.181	1.188
9	1.967E-05	1.953E-05	2.321E-05	1.180	1.188
10	1.980E-05	1.965E-05	2.335E-05	1.179	1.188
11	1.993E-05	1.977E-05	2.349E-05	1.179	1.188
12	2.006E-05	1.989E-05	2.363E-05	1.178	1.188
13	2.019E-05	2.001E-05	2.377E-05	1.177	1.188
14	2.032E-05	2.013E-05	2.391E-05	1.177	1.188
15	2.045E-05	2.025E-05	2.405E-05	1.176	1.188
16	2.058E-05	2.036E-05	2.419E-05	1.175	1.188
17	2.071E-05	2.048E-05	2.433E-05	1.175	1.188
18	2.084E-05	2.060E-05	2.447E-05	1.174	1.188
19	2.097E-05	2.072E-05	2.461E-05	1.174	1.188
20	2.110E-05	2.083E-05	2.475E-05	1.173	1.188

T [°C]	Dry air, α_{dry} [m²/s]	Saturated air, α_{sat} [m²/s]	D [m²/s]	Dry air, Le	Saturated air, Le
21	2.123E-05	2.095E-05	2.490E-05	1.172	1.188
22	2.137E-05	2.107E-05	2.504E-05	1.172	1.189
23	2.150E-05	2.118E-05	2.518E-05	1.171	1.189
24	2.163E-05	2.130E-05	2.532E-05	1.171	1.189
25	2.177E-05	2.141E-05	2.547E-05	1.170	1.190
26	2.190E-05	2.152E-05	2.561E-05	1.170	1.190
27	2.203E-05	2.163E-05	2.576E-05	1.169	1.191
28	2.217E-05	2.175E-05	2.590E-05	1.168	1.191
29	2.230E-05	2.186E-05	2.605E-05	1.168	1.192
30	2.244E-05	2.196E-05	2.619E-05	1.167	1.193
31	2.257E-05	2.207E-05	2.634E-05	1.167	1.193
32	2.271E-05	2.218E-05	2.648E-05	1.166	1.194
33	2.284E-05	2.228E-05	2.663E-05	1.166	1.195
34	2.298E-05	2.238E-05	2.678E-05	1.165	1.196
35	2.312E-05	2.249E-05	2.692E-05	1.165	1.197
36	2.325E-05	2.259E-05	2.707E-05	1.164	1.199
37	2.339E-05	2.268E-05	2.722E-05	1.164	1.200
38	2.353E-05	2.278E-05	2.737E-05	1.163	1.201
39	2.366E-05	2.287E-05	2.752E-05	1.163	1.203
40	2.380E-05	2.297E-05	2.766E-05	1.162	1.205
41	2.394E-05	2.306E-05	2.781E-05	1.162	1.206
42	2.408E-05	2.314E-05	2.796E-05	1.161	1.208
43	2.422E-05	2.323E-05	2.811E-05	1.161	1.210
44	2.436E-05	2.331E-05	2.826E-05	1.160	1.212
45	2.450E-05	2.339E-05	2.841E-05	1.160	1.215
46	2.464E-05	2.347E-05	2.856E-05	1.159	1.217
47	2.478E-05	2.355E-05	2.871E-05	1.159	1.219
48	2.492E-05	2.362E-05	2.887E-05	1.159	1.222
49	2.506E-05	2.369E-05	2.902E-05	1.158	1.225
50	2.520E-05	2.376E-05	2.917E-05	1.158	1.228
51	2.534E-05	2.382E-05	2.932E-05	1.157	1.231
52	2.548E-05	2.388E-05	2.947E-05	1.157	1.234
53	2.562E-05	2.394E-05	2.963E-05	1.156	1.238
54	2.576E-05	2.399E-05	2.978E-05	1.156	1.241
55	2.591E-05	2.404E-05	2.993E-05	1.156	1.245
56	2.605E-05	2.408E-05	3.009E-05	1.155	1.249

http://dx.doi.org/10.5772/67401

T [°C]	Dry air, α_{dry} [m²/s]	Saturated air, α_{sat} [m²/s]	D [m²/s]	Dry air, Le	Saturated air, Le
57	2.619E-05	2.412E-05	3.024E-05	1.155	1.254
58	2.633E-05	2.416E-05	3.040E-05	1.154	1.258
59	2.648E-05	2.420E-05	3.055E-05	1.154	1.263
60	2.662E-05	2.423E-05	3.071E-05	1.153	1.268
61	2.677E-05	2.425E-05	3.086E-05	1.153	1.273
62	2.691E-05	2.427E-05	3.102E-05	1.153	1.278
63	2.705E-05	2.429E-05	3.117E-05	1.152	1.284
64	2.720E-05	2.430E-05	3.133E-05	1.152	1.289
65	2.734E-05	2.431E-05	3.149E-05	1.152	1.295
66	2.749E-05	2.431E-05	3.164E-05	1.151	1.302
67	2.764E-05	2.430E-05	3.180E-05	1.151	1.309
68	2.778E-05	2.429E-05	3.196E-05	1.150	1.316
69	2.793E-05	2.428E-05	3.212E-05	1.150	1.323
70	2.807E-05	2.426E-05	3.228E-05	1.150	1.330
71	2.822E-05	2.423E-05	3.243E-05	1.149	1.338
72	2.837E-05	2.420E-05	3.259E-05	1.149	1.347
73	2.852E-05	2.417E-05	3.275E-05	1.149	1.355
74	2.866E-05	2.412E-05	3.291E-05	1.148	1.364
75	2.881E-05	2.407E-05	3.307E-05	1.148	1.374
76	2.896E-05	2.402E-05	3.323E-05	1.148	1.384
77	2.911E-05	2.395E-05	3.339E-05	1.147	1.394
78	2.926E-05	2.388E-05	3.355E-05	1.147	1.405
79	2.941E-05	2.381E-05	3.371E-05	1.147	1.416
80	2.956E-05	2.372E-05	3.388E-05	1.146	1.428
81	2.970E-05	2.363E-05	3.404E-05	1.146	1.440
82	2.985E-05	2.353E-05	3.420E-05	1.146	1.453
83	3.000E-05	2.343E-05	3.436E-05	1.145	1.467
84	3.016E-05	2.332E-05	3.453E-05	1.145	1.481
85	3.031E-05	2.319E-05	3.469E-05	1.145	1.496
86	3.046E-05	2.307E-05	3.485E-05	1.144	1.511
87	3.061E-05	2.293E-05	3.502E-05	1.144	1.527
88	3.076E-05	2.278E-05	3.518E-05	1.144	1.544
89	3.091E-05	2.263E-05	3.534E-05	1.143	1.562
90	3.106E-05	2.247E-05	3.551E-05	1.143	1.580
91	3.122E-05	2.230E-05	3.567E-05	1.143	1.600
92	3.137E-05	2.211E-05	3.584E-05	1.143	1.621

T [°C]	Dry air, α_{dry} [m²/s]	Saturated air, α_{sat} [m²/s]	D [m²/s]	Dry air, *Le*	Saturated air, *Le*
93	3.152E-05	2.192E-05	3.600E-05	1.142	1.642
94	3.167E-05	2.173E-05	3.617E-05	1.142	1.665
95	3.183E-05	2.152E-05	3.634E-05	1.142	1.689
96	3.198E-05	2.130E-05	3.650E-05	1.141	1.714
97	3.214E-05	2.107E-05	3.667E-05	1.141	1.740
98	3.229E-05	2.083E-05	3.684E-05	1.141	1.768
99	3.244E-05	2.058E-05	3.700E-05	1.141	1.798
100	3.260E-05	2.033E-05	3.717E-05	1.140	1.829

Table 4. Diffusion properties at different temperatures based on algebraic formulae in **Table 1**.

Type/name	Mathematical form	Supplemental formula(e)	Reference
Rotational energy	$G\left(\frac{1}{\lambda_r},T\right)=\frac{N_{J,\tau}}{N}=\frac{g_{J,\tau}\exp\left(-e_{J,\tau}/kT\right)}{Z_r}$	$g_{J,\tau}=\begin{cases}3(2J+1), & if \quad \tau=odd\\ 2J+1, & if \quad \tau=even\end{cases}$ $Z_r=\sum g_{J,\tau}\exp(-e_{J,\tau}/kT)$	[7]
Translational energy	$F\left(\frac{1}{\lambda_t},T\right)=\frac{dN}{Nd\left(1/\lambda_t\right)}=\frac{2}{\sqrt{\pi}}\frac{hc}{kT}\left(\frac{hc}{kT}\frac{1}{\lambda_t}\right)^{1/2}\exp\left(-\frac{hc}{kT}\frac{1}{\lambda_t}\right)$		[8]
Convolution, wave number basis	$H\left(\frac{1}{\lambda_{t,r}},T\right)=\sum_{1/\lambda_r}^{\leq 1/\lambda_{t,r}}F\left[\left(\frac{1}{\lambda_{t,r}}-\frac{1}{\lambda_r}\right),T\right]*G\left(\frac{1}{\lambda_r},T\right)$	$\int_0^\infty H_{1/\lambda_{t,r}}d(1/\lambda_{t,r})=1$	[1]
Convolution, wavelength basis	$H_{\lambda_{t,r}}=\frac{H_{1/\lambda_{t,r}}}{{\lambda_{t,r}}^2}$	$H_{1/\lambda_{t,r}}d(1/\lambda_{t,r})=-H_{\lambda_{t,r}}d\lambda_{t,r}$	
Energy release	$\Delta e=\left(e_t-\frac{3}{2}kT\right)+\left(e_{J,\tau}-\frac{3}{2}kT\right)-H_{HB}$	H_{HB} = −23324.4 J/mol	[9]
Wave number basis	$\frac{1}{\lambda}=\frac{1}{\lambda_t}+\frac{1}{\lambda_r}+\frac{1}{\lambda_{cut}}=\frac{e_t}{hc}+\frac{e_{J,\tau}}{hc}+\frac{1}{hc}(-H_{HB}-3kT)$	$\frac{1}{\lambda_{cut}}=\frac{1}{hc}(-H_{HB}-3kT)$	[1]
Evaporation flux related to absorption	$\left(N_g''\right)_{abs}=\frac{1}{2}\int_0^\infty c_{12}Y_\lambda''L_\lambda d\lambda$	$Y_{1/\lambda}''=\sum_i\int_{\omega_i}\left(\frac{I_{\lambda,i}}{hc/\lambda}\cos\theta_i\right)d\omega_i$	
Evaporation flux related to spontaneous emission	$\left(N_g''\right)_{spon}=-\int_0^\infty a_{21}Z''H_\lambda d\lambda$	$Z''=\frac{1}{4}n_g\overline{u}$, $\overline{u}=\sqrt{\frac{8kT}{\pi m_g}}$	[8]
Evaporation flux related to induced emission	$\left(N_g''\right)_{ind}=-\int_0^\infty c_{21}X_\lambda''H_\lambda d\lambda$	$X_\lambda''=\frac{1}{2}\left(n_g\pi{r_g}^2\right)\sum_i\left[\alpha r_g\int_{\omega_i}\frac{I_{\lambda,i}}{hc/\lambda}(\cos\theta_i)d\omega_i\right]$, $\alpha \sim O$ [1]	
Einstein's relation	$a_{21}\left(\frac{\overline{n_g}\,\overline{u}}{4\pi I_{b,\lambda}(hc/\lambda)^{-1}}\right)H_\lambda=c_{12}L_\lambda-c_{21}\left(\alpha\overline{n_g}\pi{r_g}^3\right)H_\lambda$	$I_{b,\lambda}=\frac{2hc^2}{e^{(hc/\lambda kT)}-1}\left(\frac{1}{\lambda}\right)^5\left[\frac{W}{m^2\text{-}sr\text{-}\mu m}\right]$	
	$I_{b,1/\lambda}=\frac{2hc^2}{e^{(hc/\lambda kT)}-1}\left(\frac{1}{\lambda}\right)^3\left[\frac{W}{m^2\text{-}sr\text{-}cm^{-1}}\right]$	$I_{b,\nu}=\frac{2h\nu^3}{c^2\left(e^{h\nu/kT}-1\right)}\left[\frac{W}{m^2\text{-}sr\text{-}s^{-1}}\right]$	

Type/name	Mathematical form	Supplemental formula(e)	Reference
Blackbody radiation intensity			
Net evaporation flux	$\left(N_g''\right)_\lambda = \frac{1}{2}\left(\frac{I_\lambda d\lambda}{hc/\lambda}\cos\theta\delta\omega\right)\left(a_{21}\frac{\overline{n_g u}}{4\pi I_{b,\lambda}(hc/\lambda)^{-1}}H_\lambda\right) - \frac{1}{2}s\left(\frac{I_{b,\lambda}d\lambda}{hc/\lambda}2\pi\right)\left(a_{21}\frac{\overline{n_g u}}{4\pi I_{b,\lambda}(hc/\lambda)^{-1}}H_\lambda\right)$	$\left\|a_{21}\left(\frac{\overline{n_g u}}{4\pi I_{b,\lambda}(hc/\lambda)^{-1}}\right)H_\lambda\right\| \gg \left\|c_{21}\left(\alpha\overline{n_g}\pi {r_g}^3\right)H_\lambda\right\|$	

Table 5. Population distribution functions for water-vapor molecules and equations related to phase-transition radiation.

2.4.2. Characteristic wavelength

Population distributions in **Figure 4** suggest the active spectral range for characteristic radiation. For T = 0–100°C characteristic wavelength peaks at 5–6 μm in the mid-IR range, which is outside the visible spectrum. **Figure 4** is a duplicate of wavelength-based population distributions $H(\lambda, T)$ in [1] for vapor molecules with respect to the transition with one hydrogen bond (*HB*) breaking/formation. The integration of the population distribution function over the entire wavelength range is unity by definition and is confirmed through numerical tests.

2.4.3. Evaporation flux equations

Phase-transition radiation involves three energy transition modes when photons interact with water molecules on the vapor-liquid interface: absorption, spontaneous emission, and induced emission. Evaporation fluxes related to these three modes for vapor molecules, N_g'' [#/m^2-s], can be associated with phase-transition radiation through (1) collision rates of water molecules and photons at the interface and (2) Einstein's coefficients. To avoid lengthy descriptions, evaporation flux equations are tabulated in **Table 5**. The spirit of these equations is that when photons interact with water molecules at the interface, there are chances for phase transitions

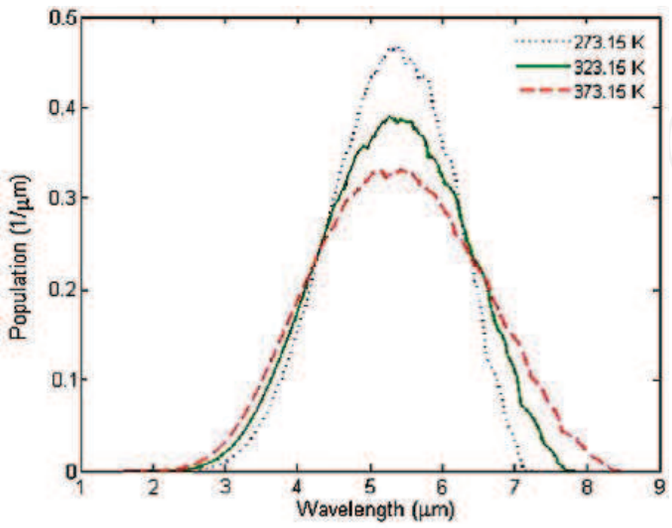

Figure 4. Population distribution functions of vapor molecules at different temperatures (duplicated from [1]).

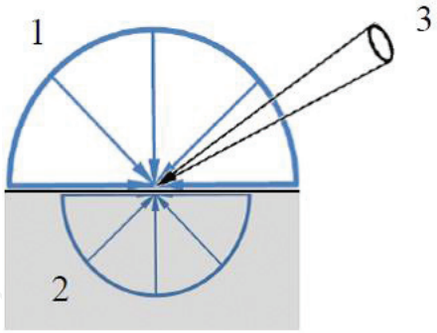

Figure 5. Different photon sources (1: external, diffuse; 2: internal, diffuse; 3: external, collimated) on the interface.

to happen. These possibilities are described as Einstein's coefficients for absorption (c_{12}), spontaneous emission (a_{21}), and induced emission (c_{21}).

Figure 5 shows three typical radiation sources on the vapor-liquid interface: (1) external diffuse-radiation $I_{\lambda,1}$; (2) internal diffuse-radiation $I_{\lambda,2}$; and (3) external collimated-radiation $I_{\lambda,3}$. Einstein's relation in **Table 5** is obtained by letting $I_{\lambda,1} = I_{\lambda,2} = I_{b,\lambda}$ (Blackbody radiation) and $I_{\lambda,3} = 0$.

2.4.4. Supersaturation by characteristic radiation

Assuming ideal gas for water vapor and using overbar to indicate saturation conditions, vapor number density n_g is related to supersaturation s via, $\boldsymbol{n_g = \overline{n_g}(1+s)}$. Saturated air with 100% relative humidity is equivalent to "zero" supersaturation.

2.4.5. Net evaporation flux

For semi-infinite water exposed to (1) Blackbody radiation $I_{b,\lambda}$ at the same temperature as water surface and (2) collimated radiation I_λ with solid angle $\delta\omega$ at angle θ (see **Figure 5** with $I_{\lambda,1} = I_{\lambda,2} = I_{b,\lambda}$ and $I_{\lambda,3} = I_\lambda$), invoking Einstein's relation, the net evaporation flux [#/m^2-s] for $\lambda \to \lambda + d\lambda$ is,

$$\begin{aligned}\left(N_g''\right)_\lambda = &\frac{1}{2}\left(\frac{I_\lambda d\lambda}{hc/\lambda}\cos\theta\delta\omega\right)\left\{\left(a_{21}\frac{\overline{n_g}\,\overline{u}}{4\pi I_{b,\lambda}(hc/\lambda)^{-1}}H_\lambda\right) - sc_{21}\left(\alpha\overline{n_g}\pi {r_g}^3\right)H_\lambda\right\} \\ &-\frac{1}{2}s\left(\frac{I_{b,\lambda}d\lambda}{hc/\lambda}2\pi\right)\left\{\left(a_{21}\frac{\overline{n_g}\,\overline{u}}{4\pi I_{b,\lambda}(hc/\lambda)^{-1}}H_\lambda\right) + c_{21}\left(\alpha\overline{n_g}\pi {r_g}^3\right)H_\lambda\right\}.\end{aligned} \tag{26}$$

The collimated radiation I_λ can be regarded as an excess radiation in addition to the background Blackbody radiation at thermodynamic equilibrium. If I_λ is taken away from Eq. (26), the net evaporation flux will automatically vanish to satisfy thermodynamic equilibrium conditions. Since s is a finite number, a simple form for evaporation flux is obtained assuming that spontaneous emission dominates the emission contribution in Einstein's relation (which is based on thermodynamic equilibrium conditions), giving,

$$\left(N_g''\right)_\lambda = \frac{1}{2}\left(\frac{I_\lambda d\lambda}{hc/\lambda}\cos\theta\delta\omega\right)\left(a_{21}\frac{\overline{n_g u}}{4\pi I_{b,\lambda}(hc/\lambda)^{-1}}H_\lambda\right) - \frac{1}{2}s\left(\frac{I_{b,\lambda}d\lambda}{hc/\lambda}2\pi\right)\left(a_{21}\frac{\overline{n_g u}}{4\pi I_{b,\lambda}(hc/\lambda)^{-1}}H_\lambda\right). \tag{27}$$

2.4.6. Supersaturation = 0

Local thermodynamic equilibrium (*LTE*) with $s = 0$ can be assumed when the collimated incident radiation I_λ is much weaker than Blackbody radiation $I_{b,\lambda}$. This leads to a much simpler form for the net evaporation flux in $\lambda \to \lambda + d\lambda$,

$$\left(N_g''\right)_\lambda = \frac{1}{2}\left(\frac{I_\lambda d\lambda}{hc/\lambda}\cos\theta\delta\omega\right)\left(a_{21}\frac{\overline{n_g u}}{4\pi I_{b,\lambda}(hc/\lambda)^{-1}}H_\lambda\right). \tag{28}$$

The resulting evaporation flux is expected to be small. The surface absorption efficiency f_s can be defined as the ratio of the net evaporation flux to the incident photon flux of the collimated radiation [6],

$$f_s = a_{21}\frac{\overline{n_g u}}{4\pi I_{b,\lambda}(hc/\lambda)^{-1}}H_\lambda\left(= \frac{a_{21}H_\lambda}{4\pi^2 I_{b,\lambda}(hc/\lambda)^{-1}}\overline{n_g}\sqrt{\frac{8\pi kT}{m_g}}\right). \tag{29}$$

Eq. (29) can also be interpreted as the fraction of radiation absorbed at interface [2].

Einstein's coefficient of spontaneous emission a_{21} is a small number on the order of 10^{-7} to 10^{-8} [10, 11]. With $a_{21} = 3 \times 10^{-8}$ [10] Eq. (29) is plotted in **Figure 6**. Readers shall not be bothered by the peaks of f_s between 2.5 and 3 μm because the evaporative flux in Eq. (28) is predominantly subject to the population distribution function H_λ.

2.4.7. Supersaturation ≠ 0

If the collimated radiation is of moderate strength (i.e., not large enough to break *LTE*), absorption of excess radiation may result in elevated evaporation flux and thus supersaturation. Eq. (27) in $\lambda \to \lambda + d\lambda$ can be written in terms of f_s,

$$\left(N_g''\right)_\lambda = \frac{1}{2}f_s\left(\frac{I_\lambda d\lambda}{hc/\lambda}\cos\theta\delta\omega\right) - \frac{1}{2}sf_s\left(\frac{I_{b,\lambda}d\lambda}{hc/\lambda}2\pi\right). \tag{30}$$

2.4.8. Quasi-steady supersaturation

Relation between supersaturation and incident radiation can be established for a thermodynamic system at quasi-steady state. Consider such a system originally at quasi-steady state without excess IR radiation to drive out water molecules from the surface and that there is neither curvature effects nor salutes to exert additional influences on equilibrium pressure. Vapor pressure at interface is just the saturation pressure at the surface temperature. As soon as an additional mid-IR radiation field is applied to the system, the evaporation rate begins to

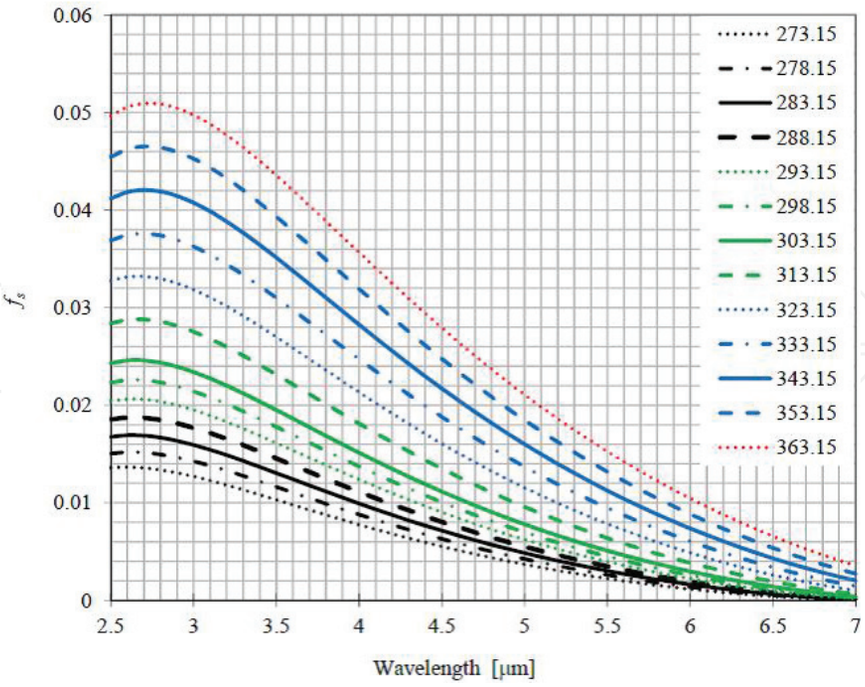

Figure 6. Surface absorption efficiency f_s.

exceed the condensation rate, and more vapor pressure starts to build up on water surface before vapor diffuses away. This is the onset of supersaturation.

As a result of the elevated vapor pressure on the surface, molecular diffusion is boosted by the increased vapor concentration gradient, leading to a higher evaporation rate. Consequently, surface temperature drops in response to the enhanced evaporation, which takes heat away from all possible sources (such as air, water, and radiation sources in all available spectral ranges) as the system tries to move toward another equilibrium state. Since saturation pressure is strongly dependent on temperature, the degree of supersaturation will be further lifted up as the surface temperature drops. Eventually supersaturation will increase to reach a new quasi-steady state at which absorption of characteristic radiation ("+" term) can no longer surpass emission ("−" term) in Eq. (30). The new quasi-steady supersaturation is assumed to be,

$$s = \frac{\cos\theta\delta\omega}{2\pi}\int_0^\infty \frac{I_\lambda}{I_{b,\lambda}} H_\lambda d\lambda, \tag{31}$$

which gives a zero evaporation flux in Eq. (30) for the integration value over the entire spectral range. Note that I_λ here is the excess radiation intensity and the quasi-steady s is independent of the probability constant a_{21}. For diffuse radiation with intensity I_λ coming from above (i.e., hemispherical radiation intensity independent of incident angle), the quasi-steady supersaturation is,

$$s = \frac{1}{2}\int_0^\infty \frac{I_\lambda}{I_{b,\lambda}} H_\lambda d\lambda. \tag{32}$$

Supersaturations caused by background Blackbody radiation with temperature T_{bkgd} is plotted in **Figure 9** following Example 5. The elevated supersaturation due to excess IR radiation

enhances evaporation by uplifting the surface vapor mass fraction, $m_{1,s}$, in Eq. (19). In distillation applications, this mechanism allows enhanced evaporation to take place below the boiling point.

In Eqs. (26)–(32), (H/I_b) is dependent on temperature but invariant with respect to the evaluation basis (wave number $1/\lambda$ or frequency ν, or even wavelength λ). To facilitate engineering analysis, coefficients for curve-fits of (H/I_b) defined in Eq. (33) are tabulated in **Table 6** for λ from 2.5 μm to the far wing where H_λ approaches zero (see **Figure 4**, generally >7.25 μm, depending on T). The units for λ and (H/I_b) in Eq. (33) are, respectively, [μm] and [cm^2-sr/W].

$$\frac{H}{I_b}\left[\frac{cm^2\text{-}sr}{W}\right] = \sum_{i=0}^{6} P(i)\left(\lambda\left[\mu m\right]\right)^i. \tag{33}$$

2.4.9. Local stability of quasi-steady supersaturation

The quasi-steady supersaturation in Eq. (31) or (32) is in favor of the local stability of the thermodynamic system. This is explained as follows. For a system already at quasi-steady state under IR characteristic radiation, a perturbation is added to the established supersaturation to examine the stability of the system. The perturbation can be either positive or negative with respect to the quasi-steady supersaturation. For a positively perturbed supersaturation, the net radiation-induced evaporation rate in Eq. (30) will become negative as a result of the slightly increased supersaturation to bring the system back to its original quasi-steady state.

T (°C)	P(6)	P(5)	P(4)	P(3)	P(2)	P(1)	P(0)
0	−1.8049E+00	7.0424E+01	−1.1017E+03	9.0590E+03	−4.1597E+04	9.8249E+04	−8.2804E+04
5	−2.3238E+00	8.2720E+01	−1.2058E+03	9.3386E+03	−4.0726E+04	9.2567E+04	−7.7111E+04
10	−1.6147E+00	5.8630E+01	−8.6986E+02	6.8497E+03	−3.0353E+04	6.9958E+04	−5.8710E+04
15	−1.1467E+00	4.2407E+01	−6.3940E+02	5.1118E+03	−2.2981E+04	5.3643E+04	−4.5323E+04
20	−8.2035E-01	3.0924E+01	−4.7402E+02	3.8482E+03	−1.7552E+04	4.1491E+04	−3.5292E+04
25	−5.9907E-01	2.2972E+01	−3.5735E+02	2.9410E+03	−1.3589E+04	3.2489E+04	−2.7806E+04
30	−4.4173E-01	1.7229E+01	−2.7193E+02	2.2681E+03	−1.0613E+04	2.5656E+04	−2.2090E+04
40	−2.4969E-01	1.0042E+01	−1.6270E+02	1.3902E+03	−6.6559E+03	1.6420E+04	−1.4297E+04
50	−1.1513E-01	5.0540E+00	−8.7390E+01	7.8839E+02	−3.9565E+03	1.0133E+04	−8.9693E+03
60	−8.4490E-02	3.6328E+00	−6.2201E+01	5.5868E+02	−2.8027E+03	7.2032E+03	−6.4134E+03
70	−4.8756E-02	2.1939E+00	−3.8903E+01	3.6015E+02	−1.8567E+03	4.8836E+03	−4.4002E+03
80	−2.8232E-02	1.3386E+00	−2.4662E+01	2.3577E+02	−1.2505E+03	3.3683E+03	−3.0713E+03
90	−1.6512E-02	8.2929E-01	−1.5903E+01	1.5708E+02	−8.5720E+02	2.3644E+03	−2.1813E+03

Table 6. Curve-fit coefficients for (H/I_b) in Eq. (33).

On the contrary, a negative perturbation for supersaturation results in a positive net radiation-induced evaporation rate to restore the system to its prior unperturbed quasi-steady state. Therefore a locally stable state is established at the quasi-steady supersaturation.

2.5. Materials and methods

The most crucial part in the engineering application of radiation-enhanced evaporation is the selection of the IR radiation source. Since the characteristic radiation is in the mid-IR spectral range, lasers and LEDs designed for this range fit in well for this purpose. However, they are not economically feasible on industrial scales. An alternative way of generating mid-IR radiation is to heat up a Blackbody-like material to a desired temperature such that the peak of its Blackbody-like radiation locates within the spectral range of characteristic radiation. Based on Wien's displacement law (λ_{max} [μm] $\times$ T [K] = 2898 [μm-K]), T = 200–300°C corresponds to λ_{max} = 6.12–5.06 μm. At T = 250°C, the corresponding λ_{max} (=5.54 μm) appears to be a preferred choice because it is near the maximums of population distributions in **Figure 4**.

Surface treatment is perhaps one of the most affordable methods to create Blackbody-like surfaces. Applying paints over surfaces can achieve this purpose because paints are usually "black" in the mid-IR spectral range. Anodized aluminum coating, which is commonly practiced in industries to passivate aluminum surfaces, is able to produce a moderately high emittance (~0.85, depending on several factors such as temperature, color, thickness, and roughness) [12] to somewhat resemble Blackbody surfaces. If there is no appearance preference in the engineering design, black color is generally recommended for surface treatment to mimic the Blackbody emittance.

As far as mass and heat transfer analysis is concerned, the temperature at water surface T_s needs to be determined before other thermal variables can be calculated. This can be done by plotting Eq. (25) in spreadsheet to visually determine T_s, as shown in Example 3. Alternatively, a computational method for computer-aided calculations is suggested in **Figure 7**. The logic behind this method for finding T_s is explained also in the same example.

2.6. Results and discussion

This section guides readers through examples to deal with water vaporization problems in distillation applications. Comments are made following the results of these examples to help readers understand methodologies presented in this chapter.

2.6.1. Example 1—isothermal water under mid-IR radiation

Consider a still lake with surface temperature T_s fixed at 20°C and a temperature gradient that vanishes at the bottom of the lake. Provided that a diffuse mid-IR radiation field with $q_{r,s}$ = 1000 W/m^2 is applied to water surface from above, estimate the maximum temperature change from its surface to the bottom due to radiative heating. Assume cloudy sky to skip solar radiation and evaporation flux, $\dot{m}'' = 10^{-4}$kg/m^2-s.

http://dx.doi.org/10.5772/67401

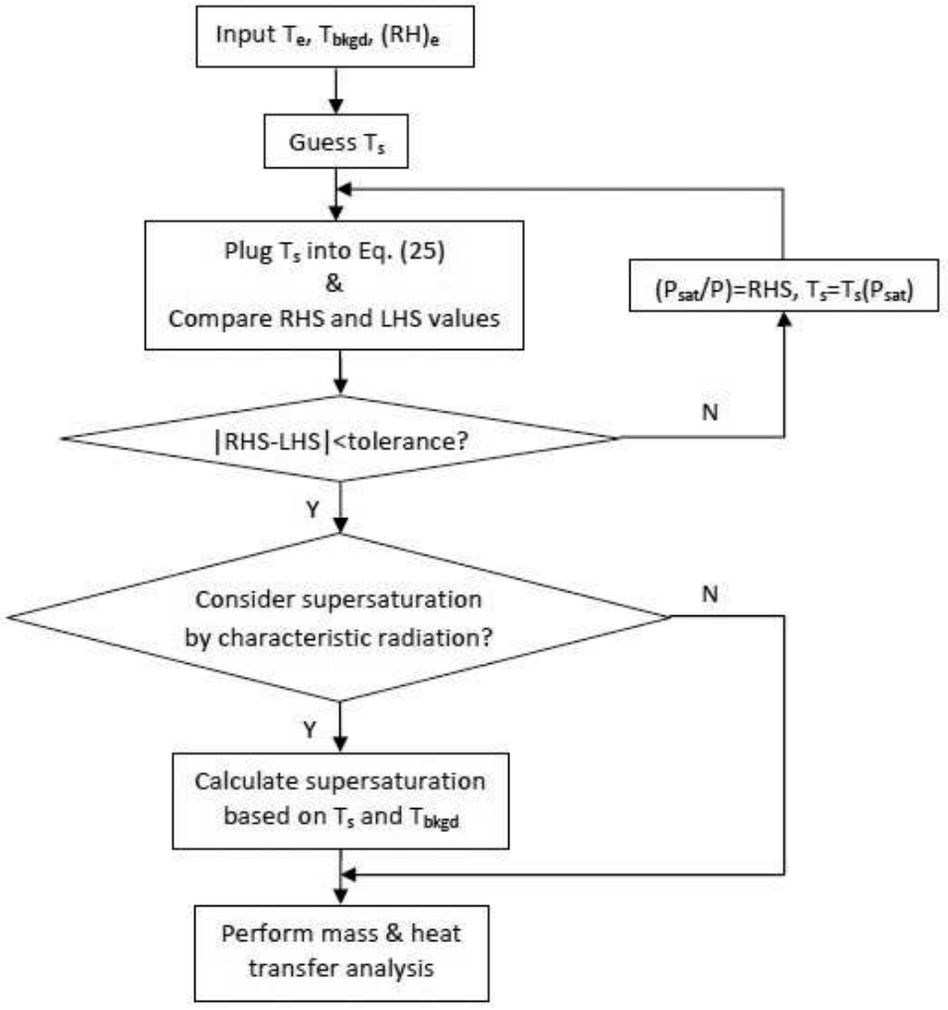

Figure 7. A flowchart for computer-aided calculations.

Solution

T_s= 20°C: k_l = 0.6 W/m-K, C= 4.2 kJ/kg-K, $\dot{m}''$= 10^{-4} kg/m^2-s => $\delta_t = k_l / (\dot{m}''C)$ = 1.42 m >> δ_r ~ 20 μm.

$0 \le f_s \le 1$, $q_{r,s}$ = 1000 W/m^2 => $\Delta T_{\max} \approx (1 - f_s) q_{r,s} \delta_r / k_l \le 0.033°C$.

$$\therefore max(T - T_s) \approx \Delta T_{\max} \left(-e^{-K_a x} + 1\right)\Big|_{x \to \infty} = \Delta T_{\max} \le 0.033°\text{C}.$$

The maximum temperature change from water surface to the bottom is estimated to be 0.033°C increase for $q_{r,s}$ = 1000 W/m^2.

This example shows that, without other heating sources, water exposed to moderate strength of mid-IR radiation is essentially isothermal at quasi-steady state. A direct conclusion of the simplified equation is that water can be treated isothermal (T_x = T_s), regardless of the value of surface absorption coefficient f_s.

For distillation applications, IR radiation sources can be designed to primarily cover the spectral range of characteristic radiation. The external IR radiation fields are intended to be

used as means to generate supersaturations instead of as major heat sources. The idea here is to apply the right amount of IR radiation in the right spectral range so that the desired supersaturation can be achieved in an economical way.

2.6.2. Example 2—economic evaluation

Given that the cost of household electricity is $0.2 USD/kWh (for example in Cambridge, Massachusetts, USA) and the desired evaporation flux is 10^{-4} kg/m^2-s, evaluate the minimum cost ($USD/Ga) for water distillation at 100°C. In the economic evaluation ignore heat loss/recovery, sensible heat for water to reach 100°C and costs related to vapor condensation and water collection.

Solution

Heat of vaporization at 100°C: 2257 kJ/kg.

Water density at 100°C: 958 kg/m^3.

Gallon to cubit meter conversion: 0.003785 m^3/Ga.

Cost per kg: $\frac{\$0.2\text{USD}}{\text{kWh}} \times \frac{2257\text{kJ}}{\text{kg}} \times \frac{\text{hour}}{3600\text{s}} = 0.125\text{USD/kg}.$

Cost per gallon: $\frac{\$0.125\text{USD}}{\text{kg}} \times \frac{958\text{kg}}{\text{m}^3} \times \frac{0.003785\text{m}^3}{\text{Ga}} = 0.453\ \ \text{USD/Ga}.$

Note that at room temperatures water density is 4% larger than that at 100°C, giving an adjusted minimum distillation cost $0.47 USD/Ga. The retail price of distilled water at Walmart (brand: Great Value Distilled Water, 1 Gal) is $0.88 USD/Ga. There are several options to reduce the production cost of distilled water: choosing a cheaper energy source, minimizing heat loss while vaporizing water, recovering heat release during vapor condensation, *or* using a new method for water vaporization such as what is proposed in this chapter.

2.6.3. Example 3—computational methods

Given that the temperature at the top of vapor layer thickness is T_e = 30°C and the corresponding relative humidity $(RH)_e$ = 0.8 and ignoring radiation effects, calculate the quasi-steady surface temperature T_s at P = 1 atm. For vapor layer thickness L = 1 mm, what is the quasi-steady evaporation flux?

Solution

2.6.3.1. Surface temperature

Since radiative heating is ignored, the isothermal approximation is applicable for liquid-water, i.e., $h_{1,o} = h_{1,u} = 4.2T_s$[°C], and there is no IR induced supersaturation, i.e., $(RH)_s = 1$.

In **Figure 2** *Le* for saturated air (*Le* ≈ 1.19) can be used because of the high relative humidity. From steam tables, $P_{sat,e}$ (T_e = 30°C) = 0.0419 atm. To begin with we shall assume a dilute system, in which $C_p \approx 1$ kJ/kg-K. The value of $m_{1,e}$ supports this assumption,

http://dx.doi.org/10.5772/67401

$$m_{1,e} \approx \frac{(0.8)(0.0419)}{1.61 - 0.61(0.8)(0.0419)} = 0.0211.$$

Eq. (25) gives,

$$\frac{P_{sat,s}}{P} \approx (0.8 \times 0.0419) + \frac{1.61}{1.19}\left[\frac{30 - T_s(^\circ C)}{2501 - 3.2T_s(^\circ C)}\right].$$

Two methods are used to obtain T_s.

Method 1: The correct value of T_s can be found by plotting the right hand side (*RHS*) and left hand side (*LHS*) values for $P_{sat,s}/P$ (based on either steam tables or **Table 1** for P_{sat}) with respect to guessed T_s in spreadsheet. The results are shown in **Figure 8**. The *LHS* curve intersects with the *RHS* to give the correct $T_s = 27^\circ C$.

Method 2: As shown in **Figure 7** the value of T_s needs to be guessed to find the corresponding $P_{sat,s}$. Plugging in the guessed T_s the *RHS* result is compared with the *LHS* for $P_{sat,s}/P$. If further guesses are needed, the *RHS* value of the present guess can be conveniently used as the *LHS* value of the new guess. This guessing method is applicable because the *RHS* and *LHS* curves come across each other at the right T_s as shown in **Figure 8**.

Saturation pressure P_{sat} and temperature T_s can be calculated using formulas for P_{sat} and T_{sat} in **Table 1**.

1st guess: $T_{sat,s} = 30^\circ C \Rightarrow P_{sat,s}/P = 0.04189 \Rightarrow RHS = 0.03353 < 0.04189 = LHS$.

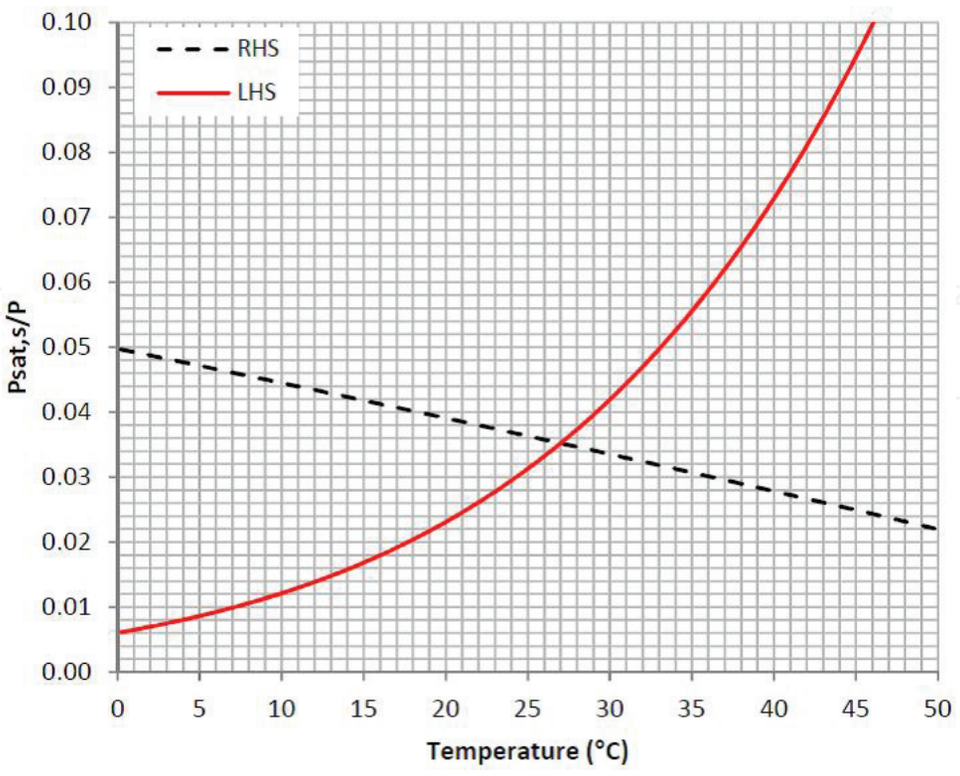

Figure 8. *RHS* and *LHS* curves for $P_{sat,s}/P$ in Example 3 with respect to guessed temperatures for T_s.

2nd guess: $P_{sat,s}/P = 0.03353 \Rightarrow T_{sat,s} = 26.18°C \Rightarrow RHS = 0.03566 < 0.03353 = LHS$.

3rd guess: $P_{sat,s}/P = 0.03566 \Rightarrow T_{sat,s} = 27.22°C \Rightarrow RHS = 0.03510 < 0.03566 = LHS$.

4th guess: $P_{sat,s}/P = 0.03510 \Rightarrow T_{sat,s} = 26.95°C \Rightarrow RHS = 0.03524 \approx 0.03510 = LHS$.

The 4th guess gives a fairly good match between *RHS* and *LHS*. For $T_s = 27°C$, the mass fraction of vapor at surface $m_{1,s}$ is 0.0222, which also supports the dilute assumption. This method seems to be tedious but becomes powerful in computer-aided computations, in which the iteration method can easily be implemented in the code.

2.6.3.2. Evaporation flux

Table 1: for $T = T_{avg} = (T_e + T_s)/2 = 28.5°C \Rightarrow \rho = 1.17\ kg/m^3$, $D = 2.60\times10^{-5}\ m^2/s$.

$$\dot{m}'' \approx \rho D \frac{m_{1,s} - m_{1,e}}{L} \approx \left(1.17 kg/m^3\right)\left(2.60 \times 10^{-5} m^2/s\right)\left(\frac{0.0222 - 0.0211}{0.001m}\right) = 3.35 \times 10^{-5} kg/m^2\text{-}s$$

The calculated T_s (=27°C) is quite close to the wet-bulb temperature for the high *RH* condition in this example. Based on the online *RH* calculator by National Weather Service Weather Forecast Office (http://www.srh.noaa.gov/epz/?n=wxcalc_rh), the web-based wet-bulb temperature is 27.13°C.

2.6.4. Example 4—enhanced evaporation by supersaturation

Following Example 3, assume that surface supersaturation can be elevated to 20% by mid-IR radiation for the isothermal liquid, and calculate the quasi-steady surface temperature and evaporation flux. Assume radiative heating in the mid-IR range can be neglected, i.e., $T_{r,s} << (T_e - T_s)$, in this example (for practical situations see Example 5).

Solution

2.6.4.1. Surface temperature

To approach the right value of T_s Eq. (25) is employed with $(RH)_s = 1.2$ and $T_{r,s} = 0$. **Table 1** is used to calculate P_{sat} and T_{sat} at surface. *Le* is approximated by 1.19 for this high *RH* system. Based on Method 2 in Example 3 (also shown in **Figure 7**), surface temperature can be evaluated to give $T_s = 24.56°C$. The quasi-steady surface temperature is brought down by ~2.5°C as compared to the saturated water surface in Example 3.

2.6.4.2. Evaporation flux

Table 3: for $T_s = 24.56°C \Rightarrow m_{1,e} = 0.0211$, $m_{1,s} = 0.0230$.

Table 1: for $T = T_{avg} = (T_e + T_s)/2 = 27.28°C \Rightarrow \rho = 1.17\ kg/m^3$, $D = 2.58\times10^{-5}\ m^2/s$.

$$\dot{m}'' \approx \rho D \frac{m_{1,s} - m_{1,e}}{L} \approx \left(1.17 kg/m^3\right)\left(2.58 \times 10^{-5} m^2/s\right)\left(\frac{0.0230 - 0.0211}{0.001m}\right) = 5.74 \times 10^{-5} kg/m^2\text{-}s$$

By boosting supersaturation to 20%, evaporation mass flux is 70% higher than that (=3.35 × 10^{-5} kg/m^2-s) in Example 3. The amount of mass flux may not seem appealing in this high *RH*

example. Nevertheless, through this pure diffusion problem it is shown that supersaturation significantly enhances evaporation.

2.6.5. Example 5—engineering application of induced supersaturation for water vaporization

Consider a still indoor pool with uniform water temperature 293.15K and the temperature of the ceiling is the same as the ambient at 303.15K. Assume Blackbody for the ceiling and water surface, and calculate the quasi-steady supersaturation and the relative humidity above vapor layer. For vapor layer thickness L = 1 mm, compute the evaporation flux and analyze how heat is supplied to liquid-water during the evaporation process. If radiation energy from the ceiling is supplied by electric heating, what is the unit cost for water vaporization based on the electricity price in Example 2 (i.e., $0.2 USD/kWh)?

Solution

2.6.5.1. Supersaturation

The quasi-steady supersaturation is evaluated using Eq. (32) with the background Blackbody temperature T_{bkgd} = 303.15K and the surface Blackbody temperature T_s = 293.15K,.

$$s = \frac{1}{2}\int_0^\infty \frac{I_{b,\lambda}\left(T_{bkgd}\right) - I_{b,\lambda}(T_s)}{I_{b,\lambda}(T_s)} H_\lambda(T_s)d\lambda. \tag{34}$$

Using **Table 5** for H_λ, the integration result for s is s = 0.185. A slightly different value of s = 0.187 is obtained based on H/I_b curve-fit values from **Table 6**.

In the midst of various sources of experimental uncertainties, the elevated supersaturation can easily be misidentified as a different thermodynamic variable such as a higher surface temperature. It is shown in the next example that, without considering Eq. (32) or (34), increasing T_s by 2°C gives s = 0 to satisfy mass and heat transfer equations at a different evaporation rate. This temperature difference (2°C) is within the accuracy range of K-type thermocouples [13].

2.6.5.2. Relative humidity

The radiation characteristic temperature $T_{r,s}$ is taken into account to solve for the value of $(RH)_e$.

Table 1: for T_{avg} = 25°C => $k = 2.59 \times 10^{-2}$ W/m-K (curve-fit coefficients in **Table 2** [5]), and

$$T_{r,s} = \frac{q_{r,s}L}{k} = \frac{\sigma\left(T_e{}^4 - T_s{}^4\right)L}{k} = \frac{60 \times 0.001}{0.0259} = 2.32 \ \ [\mathrm{K}]$$

Using Method 1 from Example 3 with $(RH)_s = 1 + s$ = 1.19 and Le = 1.19, the relative humidity above vapor layer is $(RH)_e$ = 0.49.

2.6.5.3. Mass and heat transfer

Vapor mass fractions at the s- and e-states are, respectively, $m_{1,s}$ = 0.01724 and $m_{1,e}$ = 0.01286. The dilute approximation is valid. For T_{avg} = (303.15K + 293.15K)/2 = 25°C, the corresponding evaporation flux is

$$\dot{m}'' \approx \rho D \frac{m_{1,s} - m_{1,e}}{L} \approx (1.18)\left(2.55 \times 10^{-5}\right)\left(\frac{0.01724 - 0.01286}{0.001}\right) = 1.318 \times 10^{-4}\left[\text{kg/m}^2\text{-s}\right].$$

From steam tables, heat of evaporation: h_{fg} (20°C) = 2453 [kJ/kg].

Total heat flux required for evaporation: $H_{fg} = \dot{m}'' \times h_{fg} = 323$ [W/m^2].

Since the liquid is essentially isothermal under mid-IR radiation, Eqs. (8) and (21) can be combined to give,

$$\dot{m}'' h_{fg} = -q_{c,u} + f_s q_{r,s} + k\left.\frac{dT}{dy}\right|_s = \dot{m}''(h_{1,o} - h_{1,u}) + q_{r,s} + k\left.\frac{dT}{dy}\right|_s = q_{r,s} + k\left.\frac{dT}{dy}\right|_s.$$

The conduction contribution to H_{fg} is

$$k\left.\frac{dT}{dy}\right|_s = 0.0259 \times \frac{30 - 20}{0.001} = 259\left[W/m^2\right].$$

The radiation term $q_{r,s}$ from (b) is 60 W/m^2. Most of energy required for evaporation, 80% (=259/323), is conducted from the air.

2.6.5.4. Economic evaluation

Radiation energy per unit mass: $\frac{60\text{W}}{\text{m}^2} \div \frac{1.318\times10^{-4}\text{kg}}{\text{m}^2\text{-s}} = 455.2\ \text{kJ/kg}$

Water density at 20°C: 998 kg/m^3.

Gallon to cubit meter conversion: 0.003785 m^3/Ga.

Cost per kg: $\frac{\$0.2\text{USD}}{\text{kWh}} \times \frac{455.2\text{kJ}}{\text{kg}} \times \frac{\text{hour}}{3600s} = 0.0253\ \text{USD/kg}$

Cost per gallon: $\frac{\$0.0253\text{USD}}{\text{kg}} \times \frac{998\text{kg}}{\text{m}^3} \times \frac{0.003785\text{m}^3}{\text{Ga}} = 0.096\ \text{USD/Ga}$.

As compared to Example 2, the unit cost (per gallon) for water vaporization is reduced from \$47 cents to \$10 cents. In practical engineering applications, the ceiling temperature, which reflects T_{bkgd} for the radiation source, can be different from the ambient temperature and the production volume can be scaled up by increasing water surface area.

Eq. (34) describes general situations for quasi-steady supersaturations induced by background (hemispherical) Blackbody radiation sources. **Figure 9** is constructed based on Eq. (34) to give supersaturations for some representative surface temperatures T_s and background Blackbody temperatures T_{bkgd}. It is seen in **Figure 9** that a higher T_s corresponds to a lower quasi-steady s for a fixed T_{bkgd}, which is the upper limit of T_s to give s = 0. In order to achieve s = 0.2, T_{bkgd} needs to be higher than T_s by 10.7–13.0°C respectively for T_s = 20–50°C. For a fixed T_s at 20°C, s can be uplifted from 0.2 to 0.6 by increasing T_{bkgd} from 30.7 to 46.0°C.

Note that a recommended Blackbody temperature to induce supersaturation is 250°C as discussed in Section 2.5. Since it is costly to attain such a high temperature for the entire hemispherical surface above water surface on industrial scales, a radiation source with this

http://dx.doi.org/10.5772/67401

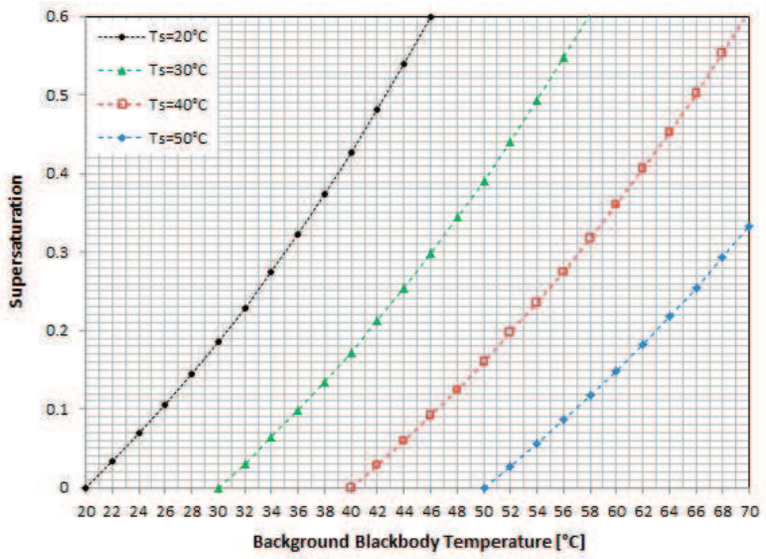

Figure 9. Quasi-steady supersaturations caused by diffuse background radiation sources characterized by Blackbody temperatures T_{bkgd} for surface temperatures T_s = 20–50°C.

temperature can be combined with other radiation sources in the engineering design. Eq. (31) can be used to integrate contributions from all radiation sources.

2.6.6. Example 6—conventional engineering analysis ignoring phase-transition radiation

Following Example 5, with the same ambient temperature, ceiling temperature, and $(RH)_e$ (=0.49), assume saturated water for the pool surface, i.e., s = 0 or $(RH)_s$ = 1, calculate the corresponding surface temperature, evaporation flux, and the amount of heat conducted from air to the pool surface. In this example the effect of characteristic radiation on supersaturation is ignored.

Solution

2.6.6.1. Surface temperature

Surface temperature T_s is expected to be slightly higher than that in Example 5 for a lower $(RH)_s$. From **Table 1**, for a slightly higher T_{avg}, a slightly higher $k = 2.6 \times 10^{-2}$ W/m-K (curve-fit coefficients in **Table 2** [5]) can be used. Using Method 1 from Example 3 with $(RH)_s$ = 1, $(RH)_e$ = 0.49, and Le = 1.19 => $T_{r,s}$ = 1.87°C and T_s = 22°C.

2.6.6.2. Mass and heat transfer

Vapor mass fractions at the s- and e-states are, respectively, $m_{1,s}$ = 0.01638 and $m_{1,e}$ = 0.01286. For T_{avg} = (30°C + 22°C)/2 = 26°C, the corresponding evaporation rate is

$$\dot{m}'' \approx \rho D \frac{m_{1,s} - m_{1,e}}{L} \approx (1.18)\left(2.56 \times 10^{-5}\right)\left(\frac{0.01638 - 0.01286}{0.001}\right) = 1.063 \times 10^{-4}\left[\text{kg/m}^2\text{-s}\right].$$

From steam tables, heat of evaporation: h_{fg} (22°C) = 2449 [kJ/kg].

Total heat flux needed for evaporation: $H_{fg} = \dot{m}'' \times h_{fg}$ = 260 [W/m^2].

The conduction contribution to H_{fg} is

$$k\frac{dT}{dy}\bigg|_s = 0.0260 \times \frac{30-22}{0.001} = 208 \ \left[\mathrm{W/m^2}\right].$$

The radiation contribution is 49 W/m^2. The evaporation flux without supersaturation drops by ~20% as compared to that in Example 5 and the amount of heat conducted/extracted from air also drops by ~20%.

3. Conclusion

For semi-infinite water under mid-IR radiation, the liquid phase is essentially isothermal as a result of the pronounced IR absorption of radiation in liquid-water. When vapor mass fraction is small compared to the air, the dilute approximation can be made and equations for mass and heat transfer can be significantly simplified. Together with these simplified forms for dilute approximations, empirical forms for thermodynamic properties are also presented in this chapter to facilitate engineering analysis.

The situation of supersaturation induced by IR characteristic radiation suggests a potential way to enhance evaporation below the boiling point. Characteristic radiation applied on the water surface directly drives water molecules out from the surface to cause evaporation. When excess IR radiation is continually applied over the surface, the quasi-steady supersaturation can be reached to enhance evaporation. Since water is nearly isothermal under mid-IR radiation with moderate radiation strength, a significant amount of heat is extracted from the air to supply the latent heat of evaporation. Blackbody-like materials heated to ~250°C can serve as mid-IR radiation sources. Economical Blackbody-like materials include black anodized aluminum surfaces and metal surfaces painted in black. With supersaturation induced by characteristic radiation in the mid-IR range, this chapter offers an economical way to enhance evaporation in distillation applications.

Acknowledgements

The second author would like to acknowledge the support of the Hermia G. Soo Professorship and NSF Grant 1457128.

Author details

Kuo-Ting Wang[1,2]*, M. Quinn Brewster[1] and Wei-Hsiang Lai[2]

*Address all correspondence to: calebuiuc@gmail.com

1 Department of Mechanical Science and Engineering, University of Illinois at Urbana-Champaign, United States

2 Department of Aeronautics and Astronautics, National Cheng Kung University, Taiwan

References

[1] Wang K.T. and Brewster M.Q. Phase-transition radiation in vapor condensation process. Int. Commun. Heat Mass Transfer. 2010;37:945–949.

[2] Brewster M.Q. Evaporation and condensation of water mist/cloud droplets with thermal radiation. Int. J. Heat Mass Transfer. 2015;88:695–712.

[3] NASA. Earth fact sheet [Internet]. Available from: http://nssdc.gsfc.nasa.gov/planetary/factsheet/earthfact.html [Accessed: Aug 2016]

[4] NOAA. Vapor pressure [Internet]. Available from: http://www.srh.noaa.gov/images/epz/wxcalc/vaporPressure.pdf [Accessed: Aug 2016]

[5] Tsilingiris P.T. Thermophysical and transport properties of humid air at temperature range between 0 and 100C. Energy Conversion and Management. 2008;49:1098–1110.

[6] Wang K.T. On Phase-Transition Radiation of Water. 1st ed. Germany: Lambert Academic Publishing; 2012. 177 p. ISBN: 978-3-659-20514-9.

[7] Randall H.M., Dennison D.M., Ginsburg N. and Weber L.R. The far infrared spectrum of water vapor. Physical Review. 1937;52:160–174.

[8] Vincenti W.G. and Kruger C.H. Jr. Introduction to Physical Gas Dynamics. New York: John Wiley and Sons, Inc.; 1965.

[9] Suresh S.J. and Naik V.M. Hydrogen bond thermodynamic properties of water from dielectric constant data. J. Chem. Phy. 2000;113(21):9727–9732.

[10] Brewster M.Q., Wang K.T., Wu W.H. and Khan M.G. Temperature effect on phase-transition radiation of water. J. Heat Transfer. 2014;136(6):062704.

[11] Wang K.T. and Brewster M.Q. Phase-change radiation: Enhanced infrared absorption in vapor-liquid water mixtures. J. Thermophys. Heat Transfer. 2013;27(3):447–457.

[12] Kauder L. Spacecraft Thermal Control Coatings References. NASA/TP. 2005; 212792.

[13] Omega. Thermocouple Reference Data [Internet]. Available from: http://www.omega.com/prodinfo/thermocouples.html [Accessed: Aug 2016]

IntechOpen